Spectroscopic properties of Er/Ce-codoped $La_3Ga_5SiO_{14}$*

Wang Qing-Guo(王庆国)[a)b)], Su Liang-Bi(苏良碧)[a)], Li Hong-Jun(李红军)[a)], Zheng Li-He(郑丽和)[a)], Xu Xiao-Dong(徐晓东)[a)], Tang Hui-Li(唐慧丽)[a)], Jiang Da-Peng(姜大朋)[a)b)], Wu Feng(吴 锋)[a)], and Xu Jun(徐 军)[a)†]

[a)] *Key Laboratory of Transparent and Opto-Functional Advanced Inorganic Materials, Shanghai Institute of Ceramics, Chinese Academy of Sciences, Shanghai* 201800, *China*

[b)] *Graduate School of the Chinese Academy of Science, Beijing* 100049, *China*

(Received 18 July 2011; revised manuscript received 16 September 2011)

The Er-single-doped and Er/Ce-codoped $La_3Ga_5SiO_{14}$ polycrystalline powders are synthesized by the solid-phase synthesis method. The room-temperature luminescence spectra of the samples are investigated. The Near-infrared-region spectroscopic properties of Er^{3+} ions in the $La_3Ga_5SiO_{14}$ systems are analysed with Judd–Ofelt theory and rate equations. The effective deactivating effect of Ce^{3+} ions on Er^{3+} ions is confirmed.

Keywords: solid-phase synthesis, spectroscopic properties, Judd–Ofelt theory, rate equation

PACS: 61.46.Hk, 61.05.cp, 74.25.Gz, 42.70.Hj **DOI:** 10.1088/1674-1056/21/2/026101

1. Introduction

Recently, rare-earth doped laser crystals attracted more and more attention. The spectroscopic properties and thermal properties of the laser crystals were reported in detail.[1−7] Laser emitting in the ∼1.5 μm spectral range has been known since 1962, when Kiss and Duncan[8] obtained oscillations in an Er-doped $CaWO_4$ crystal. Because of the broad emission at an eye-safe wavelength of ∼1.5 μm, occurring between the first excited level $^4I_{13/2}$ and the ground level $^4I_{15/2}$ of Er^{3+} ions, Er^{3+}-doped laser materials have aroused much more interest. Soon the first pulsed operation of the Er, Yb:glass laser was reported.[9]

With the development of new InGaAs laser diodes (LD) emitting at ∼980 nm, at the end of the 1980s the realization of a continuous-wave (CW) erbium laser became possible and the requirements for erbium glass were modified. CW diode-pumped operation of Er:glass laser is limited at several hundred milliwatts of output power due mainly to thermal defects inside the active element intensified by the low thermal conductivity of the glass host.[10] Because of the high thermal conductivity, erbium yttrium aluminum garnet (Er:YAG) lasers are of interest.[11] The main reason is the low branching ratio of 0.1∼0.2 for the ∼ 1.5 μm emission. According to the references, one of the methods to improve this branching ratio is co-doping with Ce^{3+} as the deactivator. Due to the phonon-assisted energy transfer between Er^{3+} and Ce^{3+} which facilitates the population of the $^4I_{13/2}$ level and simultaneously reduces up-conversion losses, the branching ratio was enhanced from 0.1∼0.2 to 0.8∼0.9.[12] In another work, the branching ratio of $^4I_{11/2} \rightarrow {}^4I_{13/2}$ transition of Er^{3+} in Er/Yb/Na/Ce:CaF_2 crystal was improved about ∼ 40 times by the deactivating effect of Ce^{3+}.[13] However it was also found that when crystals grown with several kinds of impurities, the quality and the thermal properties of the crystals became worse. Then, some host materials which contain Ce^{3+} ions were studied. For example, Yb/Er:CeF_3 nanoparticles were synthesized by hydrothermal process and its internal quantum efficiency of 1.5-μm emission reached up to 75% without visible up-conversion luminescence.[14]

Langasite (LGS, $La_3Ga_5SiO_{14}$) is a piezoelectric material that has a reasonably large piezoelectric coefficient compared with quartz crystal and belongs to the point group 32, space group $P321$. There are a few reports concerning its piezoelectric properties and

*Project supported by the National Natural Science Foundation of China (Grant Nos. 61178056 and 60938001) and the Hundred Talents Project of the Chinese Academy of Sciences.

†Corresponding author. E-mail: xujun@mail.shcnc.ac.cn

© 2012 Chinese Physical Society and IOP Publishing Ltd

surface acoustic wave (SAW) and bulk acoustic wave (BAW).[15−18] Furthermore it has excellent physical properties, such as high hardness, large specific heat, small thermal expansion and high optical transmittance and it is suited to be the laser host.[19] There are some reports on rare-earth doped LGS crystals serving as laser media and some meaningful results are obtained.[19−30]

In the present work, we prepare Er-doped and Er/Ce-codoped LGS compounds with different concentrations by the solid-phase synthesis method. Then, the spectroscopic properties of the samples are studied and the deactivating effect of Ce^{3+} ions is discussed.

2. Experiment

Twelve LGS samples were prepared by the solid-phase synthesis method. They include four Er single-doped LGS samples (Er^{3+}: 0.5 at%, 1.0 at%, 1.5 at%, and 2.0 at%; labeled as A, B, C, and D, respectively), five Er, Ce-codoped samples (CLGS, Er: 1.5 at.%; Ce:La=1:4, 1:3, 1:2, 1:1, 1:0; labeled as E, F, G, H and I, respectively) and Er, Ce, Yb-codoped samples (Er: 1.5 at%; Ce:La=1:2; Yb: 2.5 at%, 5.0 at% and 7.5 at%; labeled as J, K and L, respectively). The raw oxide materials were pressed into cylinders with a diameter of ∼20 mm after having mixed adequately. The 2 mol% over Ga_2O_3 was added into every sample due to its volatilization. Then, the pressed precursors were sintered with muffle furnace at ∼1250 °C for 12 h. Finally, we obtained the polycrystalline LGS phosphors.

The samples for spectral measurements were prepared by grinding the sintered blocks into powders. The luminescence spectra of 1000 nm∼1700 nm and 300 nm∼700 nm regions of the samples were recorded with Triax550 spectrofluorimeter under ∼980-nm LD pumping. The emission lifetimes for $^4I_{13/2}$ level and $^4I_{11/2}$ level of Er^{3+} ions were measured with a Tektronix TDS3052 digital oscilloscope to store the temporal decay curves of the fluorescence signals at ∼1530 nm and ∼1060 nm. All the measurements were taken at room temperature.

3. Results and discussion

Sample C (1.5 at% Er-single-doped LGS) was selected to be observed with scanning electron microscope (SEM). Its cross-section morphology is shown in Fig. 1. We can see the porous structure of the sintered block. The average size of the LGS powder is about 1∼2 μm.

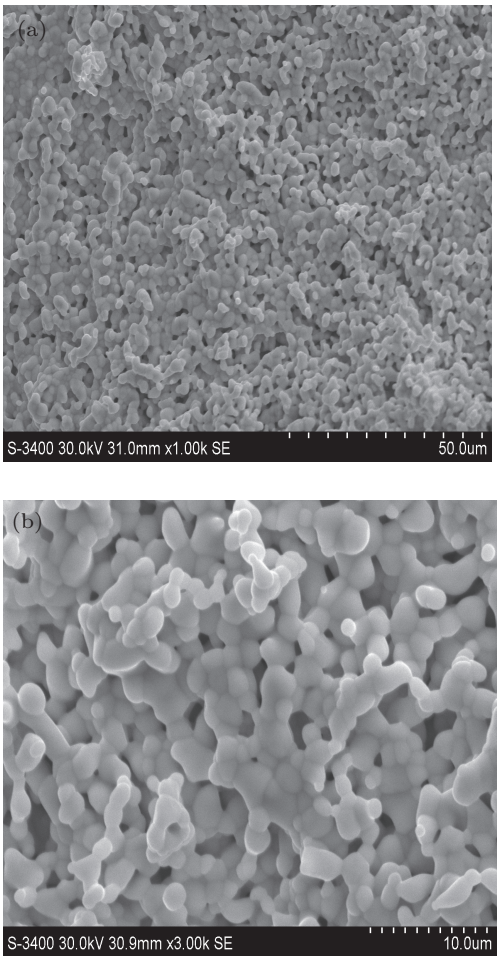


Fig. 1. The SEM images of Sample C (1.5 at% Er-doped LGS), (a) 1000×; (b) 3000×.

Figure 2 shows the X-ray diffraction (XRD) patterns of the samples C and G. From Fig. 2(a), the main

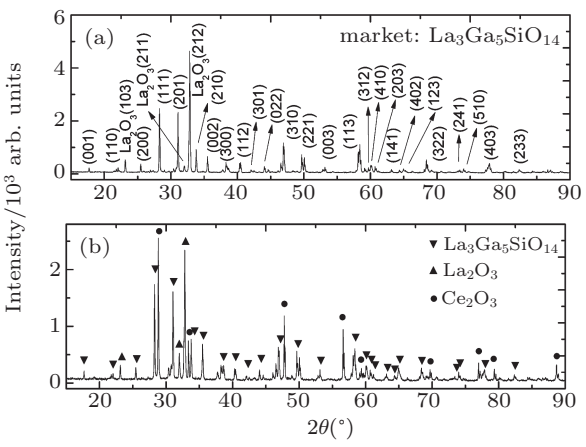


Fig. 2. XRD patterns of Er-doped LGS powder: (a) 1.5 at% Er-$La_3Ga_5SiO_{14}$ (sample C), (b) 1.5 at% Er-$(Ce_{1/3}La_{2/3})_3Ga_5SiO_{14}$ (sample G).

phase of the sample C is $La_3Ga_5SiO_{14}$ and there is also little La_2O_3 existing in it. There is no Ga_2O_3 existing in sample C. For sample G, there are only a little La_2O_3 and Ce_2O_3 powder existing in it. All the XRD measurements show that we synthesized $La_3Ga_5SiO_{14}$ particles successfully without Ga_2O_3.

Figure 3 shows the absorption, emission and transition routes of energy levels of Er^{3+} ions and the resonant energy transfer process between Er^{3+} and Ce^{3+} ions. It is shown that the energy difference (ΔE) between the $^4I_{11/2}$ level and the $^4I_{13/2}$ level of Er^{3+} is about 3600 cm^{-1}, and it is similar to that between the ground level $^2F_{5/2}$ and the $^2F_{7/2}$ level of Ce^{3+}. So, with codoping with Ce^{3+}, the decay rate of Er^{3+} $^4I_{11/2} \rightarrow {}^4I_{13/2}$ in the sample would be greatly enhanced by fast resonant energy transfer between Er^{3+} and Ce^{3+}, i.e., $(Er^{3+})^4I_{11/2} + (Ce^{3+})^2F_{5/2} \rightarrow (Er^{3+})^4I_{13/2} + (Ce^{3+})^2F_{7/2}$. It means that the branching ratio of $^4I_{13/2}$ level will be improved greatly due to the resonant energy transfer process from Er^{3+} to Ce^{3+} ions. The increase of the decay rate of $^4I_{11/2}$ level can induce the decrease of the excited state absorption (ESA) and the upconversion luminescence intensity of Er^{3+}. On the other hand, Ce^{3+} ions can also well inhibit the formation of Er–Er clusters in which the concentration-quenching could be induced due to the interaction of Er^{3+} ions.

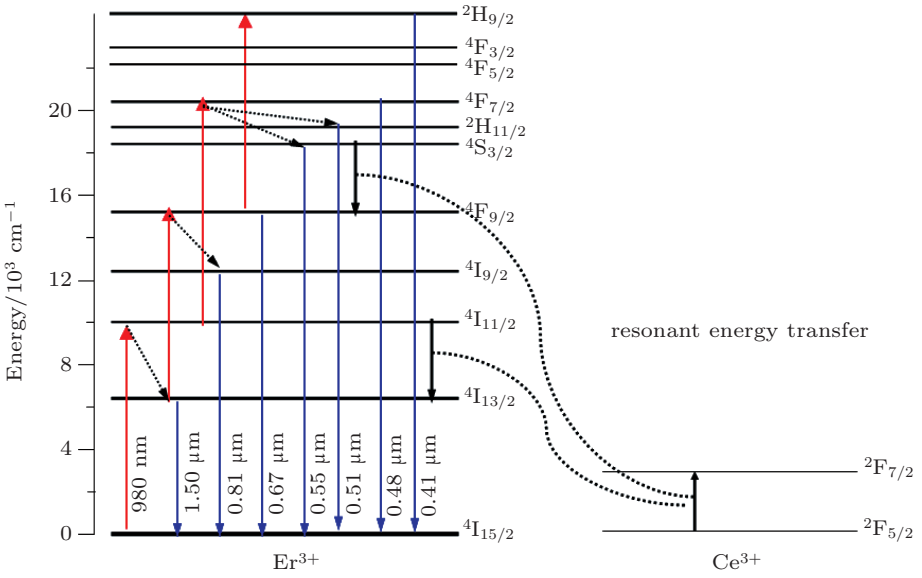


Fig. 3. (colour online) Absorption, emission transition routes of energy levels of Er^{3+} ion and the energy transfer process between Er^{3+} and Ce^{3+} ions.

Figure 4(a) shows the near-infrared (NIR) luminescence spectra of the Er single-doped LGS samples (Samples A–D) under 980-nm LD pumping. It can be seen that sample C which contains 1.5-at% Er has the highest peak luminescence intensity. When the concentration of Er^{3+} ions reaches up to 2 at%, the luminescence intensity of 1.5 μm decreases due to the interaction between the Er^{3+} ions. The cross relaxation effect between the Er^{3+} ions could increase the rate of nonradiative transition of the Er^{3+} $^4I_{13/2}$ level. With the concentration of Er^{3+} ions fixed to be 1.5 at%, Er/Ce-codoped LGS samples were synthesized in which the rate of Ce:La were 1:4, 1:3, 1:2, 1:1, and 1:0 (samples E–I), respectively. The NIR fluorescence spectra of the codoped samples are shown in Fig. 4(b). Under the same experimental conditions, the luminescence intensity of 1.5 μm first increases and then decreases and the sample G (Ce:La=1:2) has the highest luminescence intensity. The energy differences are about 6600 cm^{-1} for Er^{3+} $^4I_{13/2} \rightarrow {}^4I_{15/2}$ transition and about 3000 cm^{-1} for Ce^{3+} $^2F_{5/2} \rightarrow {}^2F_{7/2}$ transition. It just needs two Ce^{3+} ions to relax one Er^{3+} ion in the first excited state ($^4I_{13/2}$) through the following energy transfer: $^4I_{13/2}+{}^2F_{5/2} = {}^4I_{15/2}+{}^2F_{7/2}$. This process can be realized easily in the systems. So, if we increase the concentration of Ce^{3+} ions by more than 33% (Ce:La=1:2), the luminescence intensity of Er^{3+} ions at 1.5 μm will decrease. Therefore, the proper concentration of Ce^{3+} ions is important for improving the NIR luminescence

properties of Er^{3+} ions.

In order to improve the absorption efficiency of the pumping light, Yb^{3+} ions were added into the Er/Ce-codoped LGS samples with different concentrations (samples J–L). From Fig. 4(c), it can be found that the luminescence intensity of 1.5 μm increases greatly with Yb^{3+} ions codoping. Sample K (5.0% Yb^{3+}) has the highest NIR emission intensity and it is 2 times higher than that of Sample G (without Yb^{3+} codoping). The lifetimes of 1530-nm emission of the samples were obtained by fitting the corresponding decay curves (as shown in Fig. 5(a)). The lifetime of Er^{3+} $^4I_{11/2}$ level (~1060 nm) was also investigated and partly shown in Fig. 5(b). It can be seen that the lifetime of 1060 nm decreases from 582 μs (1.5% Er-single-doped LGS) to 192 μs (1.5% Er/Ce-codoped LGS, Ce:La=1:2). The lifetimes of 1060-nm emission of the Er/Ce-codoped samples are listed in Table 2. The lifetime of Er^{3+} $^4I_{11/2}$ level in 1.5% Er, 5.0% Yb-codoped CLGS (Ce:La=1:2) increases up to more than 300 μs. We think that it is because the luminescence spectrum of Er^{3+} $^4I_{11/2}$ level at 1.0 μm region overlapped with that of Yb^{3+} ions.

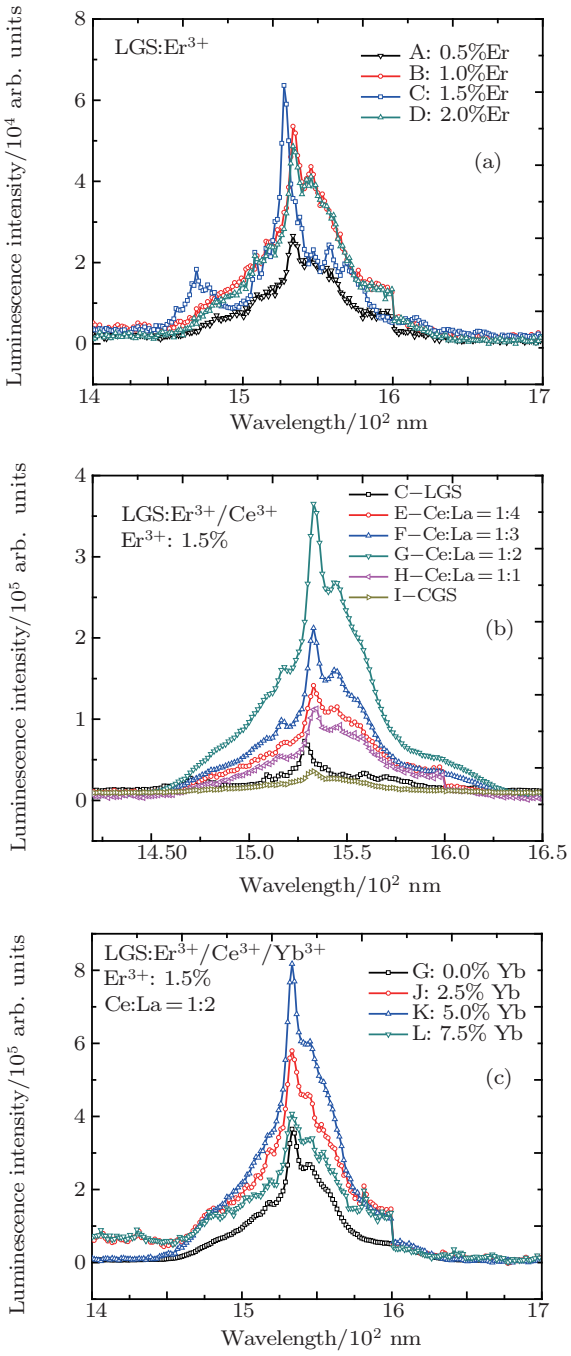


Fig. 4. (colour online) the NIR fluorescence spectra under 980-nm LD pumping for (a) Er single-doped LGS samples, (b) Er, Ce-codoped LGS samples, and (c) Er, Ce, Yb-codoped LGS samples.

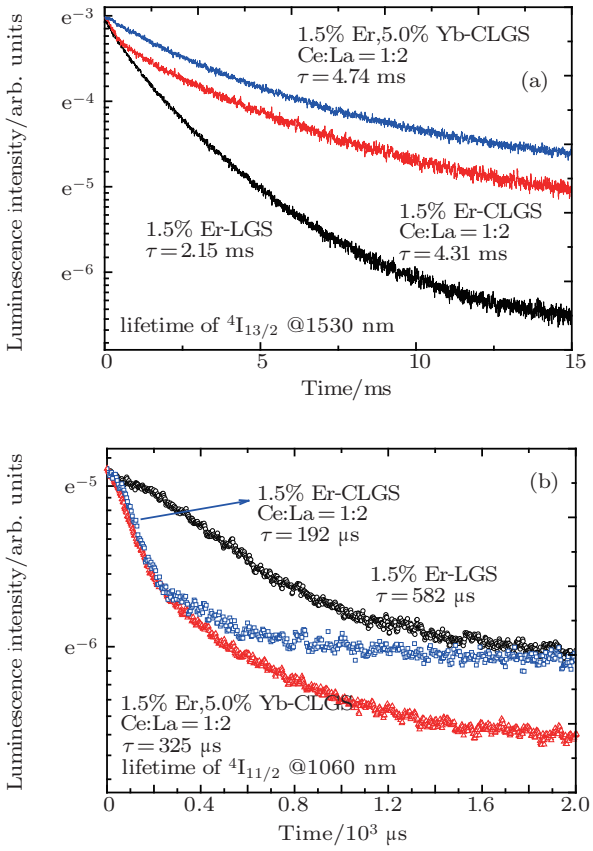


Fig. 5. (colour online) Semilog plots of Er^{3+} luminescence decay curves of Er-doped LGS samples recorded at 300 K, showing (a) lifetime of the emission of $^4I_{13/2}$ level at 1530 nm and (b) lifetime of the emission of $^4I_{11/2}$ level at 1060 nm.

The upconversion luminescence of Er^{3+} ions was investigated at 300 K under 980-nm LD pumping (as shown in Fig. 6). It can be found that the upconversion luminescence intensity of Er^{3+} ions is reduced greatly with Ce^{3+} ions codoping. But it cannot eliminate the upconversion visible luminescence of Er^{3+}

absolutely.

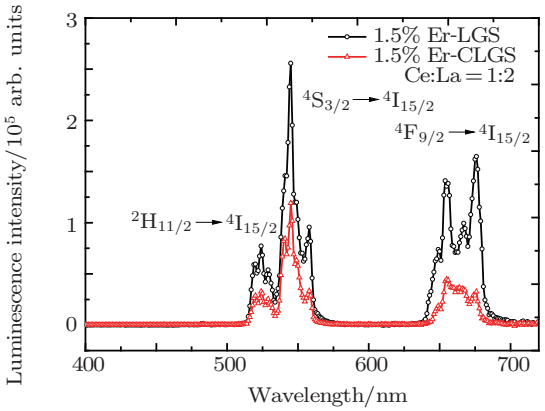


Fig. 6. (colour online) Upconversion luminescence of Er^{3+} ions in sample C (1.5% Er-single-doped LGS) and sample G (1.5% Er-CLGS, Ce:La=1:2).

Room temperature fluorescence preperties of the Er-doped LGS was analysed in the framework of the Judd–Ofelt theory[31,32] to determine radiative transition rate and luminescence branching ratio for the $^4I_{13/2}$ metastable level. According to the Judd–Ofelt theory, electronic dipole transitions within the $4f^n$ configuration of a rare-earth ion can be analysed. The electronic dipole transition line strength $S_{\rm ed}$ between two different J states can be expressed as

$$S_{\rm ed}(SLJ \rightarrow S'L'J') = \sum_{t=2,4,6} \Omega_t \left| \left\langle SLJ \left\| U^{(t)} \right\| S'L'J' \right\rangle \right|^2, \quad (1)$$

where Ω_t ($t = 2, 4, 6$) are the Judd–Ofelt parameters, S, L, J are the quantum numbers corresponding to the total spin, the total orbit and the total angular momentum, respectively, and $U^{(t)}$ are the reduced matrix elements which do not vary with host. For Er^{3+} ions, the $U^{(t)}$ can be obtained from Ref. [33]. The intensity parameters and the values $\Omega_2 = 2.74 \times 10^{-20}$ cm^2, $\Omega_4 = 0.67 \times 10^{-20}$ cm^2, and $\Omega_6 = 0.59 \times 10^{-20}$ cm^2 have been reported earlier in Ref. [19].

The radiative transition probability ($W_{\rm r}$) between the excited states can be calculated by the following expression:

$$W_{\rm r}(SLJ \rightarrow S'L'J') = \frac{64\pi^4 e^2}{3h\lambda^3(2J+1)} \times \left[\frac{n\left(n^2+2\right)^2}{9} S_{\rm ed} + n^3 S_{\rm md} \right], \quad (2)$$

where e is the charge of the electron, n is the refraction index ($n = 2.5$) and $S_{\rm md}$ is the magnetic dipole transition line strength and it can be neglected.

The fluorescence branching ratio $\beta\,(SLJ; S'L'J')$ of the transition from the excited state to the lower states and the radiative lifetime $\tau_{\rm r}$ of the initiative state can be calculate respectively with the following expressions:

$$\beta\,(SLJ \rightarrow S'L'J') = \frac{W_r(SLJ \rightarrow S'L'J')}{\sum\limits_{S'L'J'} W_r(SLJ \rightarrow S'L'J')}, \quad (3)$$

$$\tau_{\rm rad} = [\beta\,(SLJ \rightarrow S'L'J')]^{-1}. \quad (4)$$

With the intensity parameters $\Omega_{2,4,6}$ determined, the radiative transition rate $W_{\rm r}$, luminescence branching ratio β and radiative lifetime $\tau_{\rm r}$ for the $^4I_{13/2}$ level were calculated and listed in Table 1.

Table 1. Calculated values of radiative transition rate ($W_{\rm r}$), the branching ratio (β) and the radiative lifetime ($\tau_{\rm r}$) for $^4I_{13/2}$ and $^4I_{11/2}$ levels of Er-doped LGS.

Tansitions from the excited states	Transition wavelength/nm	Line strength/10^{20}	Radiative transition rate $W_{\rm r}$/s^{-1}	Branching ratio β/%	Radiative lifetime $\tau_{\rm r}$/ms
$^4I_{13/2} \rightarrow {}^4I_{15/2}$	1533	0.9767	89.3302	100	11.19
$^4I_{11/2} \rightarrow {}^4I_{15/2}$	976	0.3107	5.5713	1.57	2.81
$^4I_{13/2}$	2778	0.8461	349.8518	98.43	

The $^4I_{13/2}$ radiative lifetime defined as an inverse of the sum of radiative transition rates was found to be 11.19 ms. So, the fluorescence quantum efficiency of 1.5-μm emission was calculated to be 19.2% (1.5% Er-single-doped LGS), 38.5% (1.5% Er-doped CLGS, Ce:La=1:2), and 42.1% (1.5% Er, 5.0% Yb-codoped CLGS, Ce:La=1:2). The fluorescence quantum efficiency of $^4I_{11/2}$ level at 1060 nm was 20.7% (1.5% Er-single doped LGS), 6.83% (1.5% Er-doped CLGS, Ce:La=1:2) and 11.6% (1.5% Er, 5.0% Yb-codoped CLGS, Ce:La=1:2).

For Er/Ce-codoped LGS systems, the rate equations for the population densities in the $^4I_{11/2}$ and

$^4I_{13/2}$ states can be expressed as follows:[34]

$$\frac{dn_3}{dt} = -Kn_3 - \frac{n_3}{\tau_3}, \quad (5)$$

$$\frac{dn_2}{dt} = Kn_3 - \frac{n_2}{\tau_2}, \quad (6)$$

where n_2 and n_3 are the population densities in the $^4I_{13/2}$ state and the $^4I_{11/2}$ state, respectively; τ_2 and τ_3 are the experimental lifetimes of $^4I_{13/2}$ and $^4I_{11/2}$ levels, respectively; K is the decay rate of the $^4I_{11/2} \rightarrow {}^4I_{13/2}$ transition which was composed of two parts: the nonradiative decay rate of $^4I_{11/2}$ state for the samples without Ce^{3+}, and the energy transfer rate from Er^{3+} to Ce^{3+} ions ($K = 1/\tau_3 - 1/\tau_{3r}$, τ_{3r} is the radiative lifetime of the $^4I_{11/2}$ level). The decay rates of Er^{3+} $^4I_{11/2} \rightarrow {}^4I_{13/2}$ of the Er/Ce-codoped LGS samples were listed in Table 2.

Under the pumping of continuous LD at ∼980 nm, the dynamic equilibrium among all the populated levels is quickly reached with a stable fluorescence yield. So, we can obtain the equations as follows:

$$\frac{dn_2}{dt} = \frac{dn_3}{dt} = 0, \quad (7)$$

$$n_3 = n_{30} - C\,e^{-t/\tau_3}$$

(C is a constant which related to K), (8)

$$n_2 = \left(2K_+\frac{1}{\tau_3}\right)\tau_2 n_3. \quad (9)$$

In Er/Ce-codoped LGS samples, we assume that the n_{30} is the density of Er^{3+} ions (N). On the basis of the fluorescence integral intensity at the ∼1.5 μm, which is proportional to the populations of Er^{3+} $^4I_{13/2}$ level, i.e., $I_f(t) \propto n_2(t)$, the emission intensity of the sample at ∼1.5 μm can be estimated.

Table 2. Fluorescence properties of Er^{3+} $^4I_{11/2}$ level in the Er/Ce-codoped LGS samples.

Samples	Experimental lifetime of $^4I_{11/2}$ [τ_3/ms]	Radiative lifetime of $^4I_{11/2}$ [τ_{r3}/ms]	Decay rate of the $^4I_{11/2}\rightarrow I_{13/2}$ transition [K/s^{-1}]	Fluorescence quantum efficiency of $^4I_{11/2}$ [η/%]
C (1.5% Er-LGS)	0.582	2.81	1362	20.7
E (1.5% Er, Ce:La=1:4)	0.429	2.81	1975	15.3
F (1.5% Er, Ce:La=1:3)	0.362	2.81	2406	12.9
G (1.5% Er, Ce:La=1:2)	0.192	2.81	4852	6.8
H (1.5% Er, Ce:La=1:1)	0.374	2.81	2318	13.3
I (1.5% Er, 100% Ce)	0.544	2.81	1482	19.4

4. Conclusions

In this work, Er-single doped and Er/Ce-codoped LGS polycrystalline powders with different concentrations are synthesized by the solid-phase synthesis method. The visible upconversion and NIR luminescence spectra of the samples are investigated. It is found that 1.5 at% Er-CLGS (Ce:La=1:2) has the highest luminescence intensity at 1530 nm. The radiative lifetime of Er^{3+} $^4I_{13/2}$ ion in this system is calculated to be 11.19 ms by the Judd–Ofelt theory. The fluorescence quantum efficiency of Er^{3+} $^4I_{13/2}$ level of the sample G (1.5% Er-doped CLGS, Ce:La=1:2) reaches up to 38.5% which is 2 times more than that of 1.5% Er-single-doped LGS (19.2%). And the corresponding fluorescence quantum efficiency of Er^{3+} $^4I_{11/2}$ level decreases from 20.7% (1.5% Er-single doped LGS) to 6.8% (1.5% Er-doped CLGS, Ce:La=1:2). So that codoping with Ce^{3+} is confirmed to be an effective method to improve the quantum efficiency of Er^{3+} ∼1.5 μm radiation and to reduce the energy loss from the excited state absorption of Er^{3+}.

Acknowledgement

We would like to sincerely thank Miss Li Ya-Mei from the Shanghai Institute of Ceramics, Chinese Academy of Sciences for her assistance with SEM.

References

[1] Huang Y H, Jiang D L, Zhang J X and Lin Q L 2010 *Acta Phys. Sin.* **59** 300 (in Chinese)
[2] Yang Q H, Zhou H X and Lu S Z 2010 *Chin. Phys.* B **19** 020701
[3] Hu L, Xu X W, Lu Z M, Fan Y, Li Y X and Tang C C 2010 *Chin. Phys.* B **19** 127807
[4] Xie W, Wang Y H, Hu Y H, Wu H Y, Deng L Y and Liao F 2010 *Acta Phys. Sin.* **59** 1148 (in Chinese)

[5] Xie W, Wang Y H, Hu Y H, Luo L, Wu H Y and Deng L Y 2010 *Acta Phys. Sin.* **59** 3344 (in Chinese)
[6] Yang Z P, Ma X, Zhao P P and Song Z F 2010 *Acta Phys. Sin.* **59** 5387 (in Chinese)
[7] Wang D G, Zhou Y X, Wang X S, Dai S X, Shen X, Chen F F and Wang S 2010 *Acta Phys. Sin.* **59** 6256 (in Chinese)
[8] Kiss Z J and Duncan R C 1962 *Rroc. IEEE* **50** 1531
[9] Snitzer E and Woodcock R 1965 *Appl. Phys. Lett.* **6** 45
[10] Tolstik N A, Kisel V E, Kuleshov N V and Maltsev V V 2009 *Appl. Phys.* B **97** 357
[11] Yu Y Q, Wu Z J and Zhang S Y 2000 *J. Alloys Compd.* **302** 204
[12] Meng Z, Yoshimura T, Fukue K, Higashihata M, Nakata Y and Okada T 2000 *J. Appl. Phys.* **88** 2187
[13] Xu J, Su L B, Li H J, Zhang D, Wen L, Lin H and Zhao G J 2007 *Opt. Mater.* **29** 932
[14] Tan M C, Kumar G A and Riman R E 2009 *Opt. Express* **17** 15904
[15] Jung I H, Ko J M, Shim K B, Fukuda T and Auh K H 2000 *J. Cryst. Growth* **220** 275
[16] Jung I H and Auh K H 1999 *Mater. Lett.* **41** 241
[17] Jung I H, Fukuda T and Auh K H 2002 *J. Ceram. Process. Res.* **3** 6
[18] Takeda H, Kato T, Chani V I, Morikoshi H, Shimamura K and Fukuda T 1999 *J. Alloys Compd.* **290** 79
[19] Wang Z M, Liu Y C, Yin Y S and Yuan D R 2006 *Cryst. Res. Technol.* **41** 1142
[20] Wang Z M, Yuan D R, Shi X Z, Cheng X F, Xu D, Lü M K, Pan L H and Guo S Y 2003 *J. Cryst. Growth* **257** 141
[21] Wang Z M, Yuan D R, Xu D, Lü M K, Cheng X F, Pan L H and Shi X Z 2003 *J. Cryst. Growth* **255** 348
[22] Wang Z M, Yin Y S and Yuan D R 2006 *Appl. Phys.* A **85** 437
[23] Wang Z M, Yin Y S and Yuan D R 2007 *J. Alloys. Compd.* **436** 364
[24] Wang Z M, Yuan D R, Shi X Z, Cheng X F, Xu D, Lü M K and Pan L H 2004 *J. Cryst. Growth* **263** 246
[25] Georgescu S, Toma O, Chinie A M, Gheorghe L, Achim A and Stefan A S 2008 *Opt. Mater.* **30** 1007
[26] Georgescu S, Toma O, Chinie A M, Gheorghe L, Achim A and Stefan A S 2008 *J. Lumin.* **128** 741
[27] Georgescu S, Voiculescu A M, Toma C M O, Gheorghe L and Achim A 2010 *Romamian Reports in Physics* **62** 128
[28] Ren Y Y, Tan Y, Chen F, Jaque D, Zhang H J, Wang J Y and Lu Q M 2010 *Opt. Express* **18** 16258
[29] Burkov V I, Lysenko O A and Mill B N 2010 *Phys. Crystallography Reports* **55** 983
[30] Kim Y S and Auh K H 2002 *Mater. Lett.* **57** 28
[31] Judd B R 1962 *Phys. Rev.* **127** 750
[32] Ofelt G S 1962 *J. Chem. Phys.* **37** 511
[33] Kumar G A, Riman R, Chae S C, Jang Y N, Bae I K and Moon H S 2004 *J. Appl. Phys.* **95** 3243
[34] Meng Z, Yoshimura T, Fukue K, Higashihata M, Nakata Y and Okada T 2000 *J. Appl. Phys.* **88** 2187